EurJIC
European Journal of Inorganic Chemistry

Chemistry Europe
European Chemical Societies Publishing

Accepted Article

Title: Oxygen Transfer from Trimethylamine N-oxide to CuI Complexes Supported by Pentanitrogen Ligands

Authors: Erick Ramírez, Md. Kamal Hossain, Marcos Flores-Alamo, Matti Haukka, Ebbe Nordlander, and Ivan Castillo

To be cited as: *Eur. J. Inorg. Chem.* 10.1002/ejic.202000488

Link to VoR: https://doi.org/10.1002/ejic.202000488

WILEY-VCH

10.1002/ejic.202000488

WILEY-VCH

FULL PAPER

Oxygen Transfer from Trimethylamine N-oxide to Cu^{I} Complexes Supported by Pentanitrogen Ligands

Erick Ramírez,[a] Md. Kamal Hossain,[b] Marcos Flores-Alamo,[c] Matti Haukka,[d] Ebbe Nordlander,[b] Ivan Castillo*[a]

[a] M.Sc. E. Ramírez, Dr. I. Castillo
Instituto de Química
Universidad Nacional Autónoma de México
Circuito Exterior, CU, 04510, México
E-mail: joseivan@unam.mx
https://iquimica.unam.mx/dr-ivan-castillo-perez
[b] Md. K. Hossain, Dr. E. Nordlander
Chemical Physics
Center for Chemistry and Chemical Engineering, Lund University
Box 124, SE-221 00 Lund, Sweden
[c] Dr. Marcos Flores-Alamo
Facultad de Química, División de Estudios de Posgrado
Universidad Nacional Autónoma de México
Circuito Exterior, CU, 04510, México
[d] Dr. Matti Haukka
Department of Chemistry
University of Jyväskylä
P.O. Box-35, Jyväskylä, FI-40014, Finland

Supporting information for this article is given via a link at the end of the document.

Abstract: [*N*,*N*-bis(1-methyl-2-benzimidazolyl)methyl-*N*-(bis-2-pyridylmethyl)amine] (**L_1**) and [*N*,*N*-bis(2-quinolylmethyl)-*N*-bis(2-pyridyl)methylamine] (**L_2**) were employed to prepare Cu^{II} and Cu^{I} complexes for spectroscopic and structural characterization. [**L_1**$Cu^{II}(H_2O)](NO_3)_2$ and [**L_2**$Cu^{II}(NO_3)]NO_3$ have Jahn-Teller distorted octahedral geometries, and give rise to isotropic EPR spectra in frozen solution. [**L_1**$Cu^{I}(CH_3CN)]OTf$ and [**L_2**$Cu^{I}(CH_3CN)]OTf$ have distorted trigonal bipyramidal and tetrahedral solid-state structures, respectively. The *N*-donors display labile behavior in solution, based on variable-temperature $_1$H NMR studies. Addition of trimethylamine *N*-oxide (Me_3NO) to solutions of [**L_1**$Cu^{I}(CH_3CN)]OTf$ and [**L_2**$Cu^{I}(CH_3CN)]OTf$ resulted in diamagnetic species tentatively assigned as the corresponding adducts upon replacement of coordinated acetonitrile, based on $_1$H NMR spectroscopy. Heating [**L_1**$Cu^{I}(CH_3CN)]OTf$ to 50-60°C in the presence of Me_3NO resulted in its cupric analogue [**L_1**$Cu^{II}(CH_3CN)]^{2+}$, as well as a small amount of 2-dipyridylketone, along with other oxidation byproducts. In the case of [**L_2**$Cu^{I}(CH_3CN)]OTf$, the reaction with Me_3NO resulted in the cupric complex bis(2-quinolinecarboxamidato)copper(II), along with 2-dipyridylketone as oxidation products.

Introduction

The elusive intermediates of copper-based oxidative enzymes are of great interest, not only for their potential use in organic synthesis, but also to understand the fundamental properties of copper-oxygen entities as reactive species.[1] Polypyridine ligands have been employed in the most widespread approach to mimic these types of enzymes.[2] However, ligands containing donor moieties with more steric hindrance and different sigma donor ability have received considerably less attention. In this regard, the preparation of copper complexes with benzimidazole and quinoline-based N5-donor ligands is of general interest,[3,4] and in particular for our research group.

Cupric-superoxo ($CuO_2^{\cdot-}$) intermediates have been proposed as the first step in copper-based enzymatic oxygen activation, although calculations predict that the cupryl species (CuO^{+}) should be more reactive for C-H bond activation.[5] While cupryl intermediates have been invoked in monooxygenase enzymes, attempts to identify the putative *Cu-oxyl* unit (Cu^{n+}-$O^{\cdot-}$) have not succeeded thus far.[6] This is partly due to the difficulty of cleanly achieving the O-O bond cleavage that would lead to CuO^{+} from dioxygen or peroxides. Gas-phase studies have led to the proposal that the electronic structure in the putative $[(CH_3CN)CuO]^{+}$ species consists mostly of contributions from a copper(I)-biradical oxygen (Cu^{+}-O:), and a copper(II)-oxyl radical structure (Cu^{2+}-$O^{\cdot-}$).[7] A higher hydrogen atom-abstraction ability is predicted from the form with biradical character.

Despite the fact that reactions of copper(I) complexes with *N*-oxides could lead to oxygen transfer from nitrogen to copper, thus avoiding the O-O cleavage step, these transformations have not been extensively studied. The group of Maumy reported the ligand oxidation of Cu(I) and Cu(II) benzylic alcoholates and diaryl acetic carboxylates using Me_3NO; they attributed the two and four electron oxidations observed to the formation of a cupryl intermediate.[8] The mechanisms proposed proceed either by oxene transfer from Me_3NO in the case of the copper(I) complexes, or via anionic oxygen atom transfer and loss of $Me_3N^{\cdot+}$

(Scheme 1). On the other hand, Tolman and coworkers have investigated the formation of a number of copper(I) N-oxide adducts, and a bis(μ-oxido)dicopper complex obtained with oxygen transfer reagents like PhIO, pyridine-*N*-oxides or Me_3NO.[9] A recent study by the group of Karlin with aniline *N*-oxides suggests that the oxygen transfer to copper(I) complexes with pyridine and amine donors yields LCu^{II}-O· intermediates that are proposed as the active species in the activation of the strong C-H bonds (~90 kcal/mol) of the same anilines as substrates; a number of oxidation products were characterized and a plausible mechanism based on trapped experiments was proposed.[10] Oxygen transfer appears to be the rate limiting step, while higher redox potentials of the $Cu^{II/I}$ couples result in higher yields.

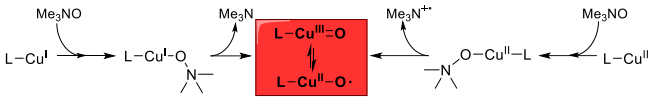

Scheme 1. Adduct formation with Me_3NO followed by oxene or oxido transfer to form the putative Cu(II)-oxyl intermediate.

Metal-oxido complexes with pyridine-based ligands are known for Mn, Fe, and V;[11] these complexes are stabilized in high oxidation states due to the donor ability of the ligands, and the possibility to form metal-oxygen multiple bonds. However, for transition metals with high *d* electron counts, the metal complexes become unstable, favoring the elimination of H_2O_2 or O_2. Copper is among such metals that lie on the right hand (forbidden) side of the *oxo-wall*,[11] making the putative copper-oxyl complexes highly reactive and likely relevant in the activation of strong C-H bonds. In this context, we herein describe the reactivity of copper complexes with *N*-based pentadentate ligands toward trimethyl *N*-oxide (Me_3NO), providing evidence of adduct formation, and oxygen-transfer to copper resulting in both intra- and intermolecular C-H activations.

Results and Discussion

Synthesis, characterization, structural analysis, and reactivity of copper(II) and copper(I) complexes

Copper(II) complexes were obtained from the reactions of cupric nitrate trihydrate and ligands [*N*,*N*-bis(1-methyl-2-benzimidazolyl)methyl-*N*-(bis-2-pyridylmethyl)amine] (**L₁**) and [*N*,*N*-bis(2-quinolylmethyl)-*N*-bis(2-pyridyl)methylamine] (**L₂**, Figure 1) in equimolar amounts in a minimum amount of acetonitrile at ambient temperature. Crystals of $[\mathbf{L_1}Cu^{II}(H_2O)](NO_3)_2$ and $[\mathbf{L_2}Cu^{II}(NO_3)]NO_3$ suitable for characterization by X-ray diffraction were obtained by vapor diffusion of ethyl acetate into an acetonitrile solution for five days. Both complexes were isolated as air-stable solids. The Cu(I) complexes were likewise synthesized by mixing **L₁** and **L₂** with $[Cu(CH_3CN)_4]OTf$ in anhydrous acetonitrile under inert atmosphere, and were isolated by crystallization from the reaction mixtures. The complexes were obtained as yellow and orange crystals suitable for X-ray analysis.

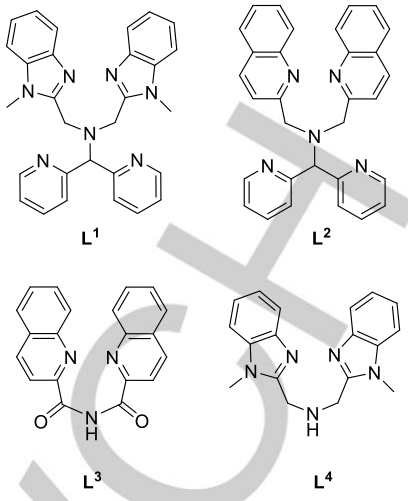

Figure 1. Structure of ligands *[N-bis(1-methyl-2-benzimidazolyl)methyl-N-(bis-2-pyridylmethyl)amine]* (**L₁**) and *[N,N-bis(2-quinolylmethyl)-N-bis(2-pyridyl)methylamine]* (**L₂**), and oxidation byproducts *2-quinolinecarboxamide* (**L₃**), *1H-benzimidazole-2-methanamine* (**L₄**).

Solid-state structures

The cupric complex $[\mathbf{L_1}Cu^{II}(H_2O)](NO_3)_2$ crystallizes in the monoclinic space group $P2_1/c$. The monometallic complex presents an elongated pseudo-octahedral geometry with all the heterocyclic nitrogen donors in the equatorial positions, and the central amine as well as a water molecule in the axial positions (Figure 2). Bond distances in the equatorial plane are quite similar, ranging from 1.970(2) Å (Cu1-N1) to 2.119(2) Å (Cu1-N5), while the N-atom in the apical position has the longest Cu-N distance at 2.376(2) Å. The longer Cu-N and Cu-O distances can be attributed to a Jahn-Teller distortion for the d_9 Cu(II) ion. This contrasts with the structure of the quinoline cupric analog $[\mathbf{L_2}Cu^{II}(NO_3)]NO_3$, where the longest Cu-N distance corresponds to one of the pyridine N-atoms, followed by that to the quinoline-derived N3 atom. This complex also crystallizes as a distorted octahedron in the triclinic space group *P*-1. Two independent cations $[\mathbf{L_2}Cu^{II}(NO_3)]_+$ are present in the asymmetric unit, one of them is shown Figure 2. The solid-state structure of this complex was previously reported in the monoclinic space group $P2/a$,[3] with small differences in the bond distances; the most significant difference corresponds to the Cu1-N5 distance (2.572(3) Å), which is the only one that is longer than the previously reported one at 2.534(2) Å, and is also a reflection of Jahn-Teller distortion. The metric parameters described for $[\mathbf{L_2}Cu^{II}(NO_3)]_+$, with the long axial Cu-N3 and Cu-N5 distances, agree with a 4 + 2 coordination mode in related compounds.[12] Insofar as the bond angles are concerned, there are no significant differences.

10.1002/ejic.202000488

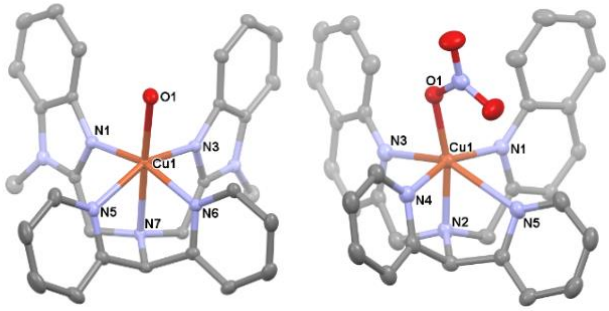

Figure 2. Mercury diagrams of [**L**$_1$Cu^{II}(H$_2$O)](NO$_3$)$_2$ (left), and [**L**$_2$Cu^{II}(NO$_3$)]NO$_3$[3] (right) at the 50% probability level; H atoms, solvent molecules, and anions are omitted for clarity.

The axial elongation of the Cu1-N7 bond in [**L**$_1$Cu^{II}(H$_2$O)](NO$_3$)$_2$, may be attributed to the methylene-C-N angles in the metallacycles formed with benzimidazole groups compared to the quinoline analogs.[4],[13],[14] The wider C-C-N angles of 124.1(2)° and 123.2(2)° may cause the elongation to reduce the strain in the five-membered rings of [**L**$_1$Cu^{II}(H$_2$O)](NO$_3$)$_2$, which contrasts with the 117.2(3)° and 120.6(3)° C-C-N angles in [**L**$_2$Cu(NO$_3$)]NO$_3$. This is also reflected in the elongated vs compressed octahedral deformations observed, which may also be reflected in the higher reactivity of the quinoline-based [**L**$_2$Cu^{I}(CH$_3$CN)]OTf (see below). In terms of basicity of the *N*-donors, the benzimidazole group should induce a greater *trans* influence towards the pyridine nitrogen than quinoline, although the steric effect appears to dominate.[14] This is reflected in the distortion of the N$_{amine}$-Cu-O angle of [**L**$_1$Cu^{II}(H$_2$O)](NO$_3$)$_2$ (178.51(6)°), relative to that of [**L**$_2$Cu^{II}(NO$_3$)]NO$_3$ (167.3(1)°). The deviation from the straight angle may be caused by the shorter H$_{quinoline}$...O$_{nitrate}$ distances, which range from 2.255 to 2.471 Å vs the H$_{benzimidazole}$...O$_{water}$ distances 2.630 and 2.714 Å.

Regarding the corresponding Cu(I) complexes, [**L**$_1$Cu^{I}(CH$_3$CN)]OTf crystallizes as a monometallic complex in the triclinic space group *P*-1. The geometry around the Cu(I) center is *pseudo*-trigonal bipyramidal for both crystallographically independent monomers in the asymmetric unit, where the central amine, two benzimidazoles, one pyridine, and one acetonitrile molecule are coordinated; the two units are similar in terms of bond distances and angles, except for the Cu-N distance to the central amine, see below. The other difference is the orientation of the free pyridine (Figure 3). Bond distances between the pyridine nitrogen and copper ions are virtually identical at 2.165(5) and 2.168(5) Å, but the benzimidazole nitrogen-copper distances are slightly different at 2.043(5) Å for Cu2-N9 and 2.086(4) Å for Cu1-N1. Finally, the distances between the acetonitrile N-atom and Cu(I) ions are identical at 1.978(6) Å. The Cu-N interactions with the central amine appear to be weak, based on the distances of 2.702(5) and 2.602(5) Å. The observed distances follow the trend expected for the hybridization at the nitrogen atoms.

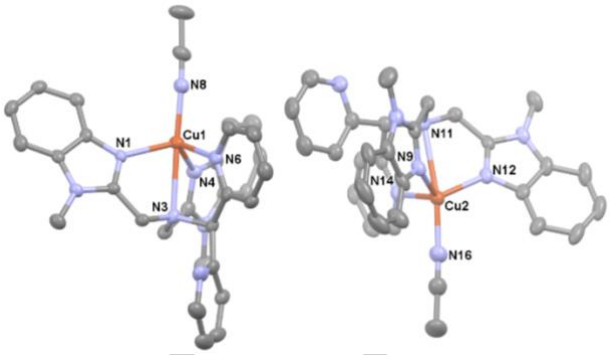

Figure 3. Mercury diagram of the two crystallographically independent [**L**$_1$Cu^{I}(CH$_3$CN)]$_+$ at the 50% probability level; H atoms, solvent molecules, and triflate anions are omitted for clarity.

In contrast, [**L**$_2$Cu^{I}(CH$_3$CN)]OTf crystallizes in the triclinic space group *P*-1, but with only one monomeric species in the asymmetric unit (Figure 4). Two quinolines, the central amine, and one acetonitrile molecule are bound to the Cu(I) center. This may be considered to be an expected result based on electronic considerations, due to the lower basicity of the quinoline moiety in acetonitrile, which stabilizes the soft cuprous ion better than pyridine (pKa values in acetonitrile: 11.96 and 12.53, respectively).[15] The geometry of the copper ion is distorted tetrahedral, the Cu-N distance to acetonitrile is the shortest among the copper and nitrogen donors [1.903(3) Å], followed by the distances towards the quinoline nitrogen atoms [2.056(3) and 2.046(2) Å]; the Cu-N distance to the central amine is the longest at 2.213(3) Å, again consistent with formal hybridization at nitrogen.

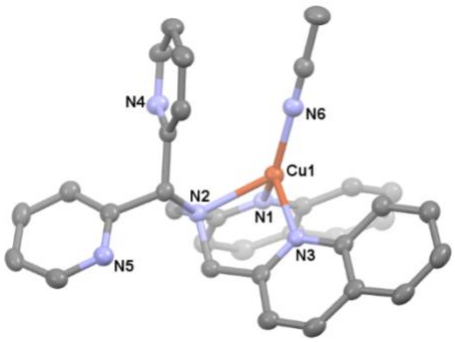

Figure 4. Mercury Diagram of [**L**$_2$Cu^{I}(CH$_3$CN)]$_+$ at the 50% probability level; hydrogen atoms, solvent molecules, and triflate anions are omitted for clarity.

Solutions of [**L**$_1$Cu^{I}(CH$_3$CN)]OTf and [**L**$_2$Cu^{I}(CH$_3$CN)]OTf were tested for dioxygen reactivity in dry and degassed THF and acetonitrile at -80°C and -30°C, respectively. No sign of oxidation of the Cu(I) complexes was evident under those conditions by UV-vis spectroscopy. Exposure to dioxygen at room temperature resulted in slow reactions, based on the color of the solutions after a few days. Indeed, both complexes are stable to air for days in the solid state. In the case of [**L**$_2$CuI(CH$_3$CN)]OTf, exposure to air for extended periods of time in THF solution afforded brown crystals of bis(2-quinolinecarboxamidato)copper(II) [(**L**$_3$)$_2$Cu^{II}] in Figure 5 (**L**$_3$ = 2-quinolinecarboxamide), in 20% isolated yield. This complex has been reported recently by Tolman and

coworkers,[16] although in that case it was obtained from a Cu(I) carboxamide dimer. Both solid-state structures share the *C*2/*c* space group, although with different cell parameters. The differences in the packing are reflected only in the N1-Cu-N1' (157.53°) and N3-Cu-N3' (158.51°) angles reported herein, relative to those previously reported at 155.4° and 159.4°, respectively. A Jahn-Teller distortion is reflected in the elongated Cu1-N1 (and symmetry-generated Cu1-N1') distances of 2.297 Å. Similar methylene group oxidations have been observed with Cu(II), Fe(III), and Co(III) in the presence of O_2.[17],[18],[19]

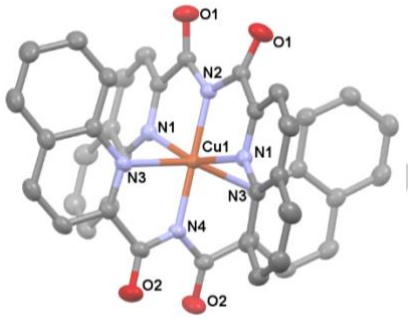

Figure 5. Mercury diagram of [(**L**$_3$)$_2$Cu^{II}] at the 50% probability level; H atoms omitted for clarity.

Table 1. Selected bond distances [Å] and angles [°].

			Distances			
[**L**$_1$Cu^{II}(H$_2$O)](NO$_3$)$_2$	[**L**$_2$Cu^{II}(NO$_3$)]NO$_3$	[**L**$_1$Cu^{I}(CH$_3$CN)]OTf	[**L**$_2$Cu^{I}(CH$_3$CN)]OTf	[(**L**$_3$)$_2$Cu^{II}]	[**L**$_1$Cu^{II}(CH$_3$CN)]OTf$_2$	[**L**$_4$Cu^{II}(OTf)$_2$(H$_2$O)]
Cu-N1 1.970(2)	Cu-N1 2.082(3)	Cu1-N1 2.086(4)	Cu-N1 2.046(2)	Cu-N1 2.297(2)	Cu-N1 2.034(2)	Cu-N1 1.972(4)
Cu-N3 2.048(2)	Cu-N2 2.037(3)	Cu1-N3 2.603(5)	Cu-N2 2.213(3)	Cu-N2 1.942(2)	Cu-N3 2.351(2)	Cu-N3 2.032(5)
Cu-N5 2.120(2)	Cu-N3 2.433(3)	Cu1-N4 2.049(5)	Cu-N3 2.056(3)	Cu-N3 2.286(2)	Cu-N4 2.000(2)	Cu-N4 1.991(4)
Cu-N6 2.021(2)	Cu-N4 2.029(3)	Cu1-N6 2.165(5)	Cu-N6 1.904(3)	Cu-N4 1.932(2)	Cu-N6 2.090(2)	Cu-O7 1.926(4)
Cu-N7 2.376(2)	Cu-N5 2.572(3)	Cu1-N8 1.978(5)			Cu-N7 2.052(2)	
Cu-O1 2.186(1)	Cu-O1 1.965(2)				Cu-N8 2.179(2)	
			Angles			
N1-Cu-N6 159.65(6)	O1-Cu-N2 168.22(10)	N4-Cu1-N1 113.51(18)	N1-Cu-N3 107.40(10)	N2-Cu-N3 100.75(5)	N4-Cu-N1 88.87(7)	N1-Cu-N(4) 164.4(2)
N1-Cu-N3 87.77(6)	N4-Cu-N2 80.64(11)	N8-Cu1-N6 105.0(2)	N6-Cu-N2 127.68(11)	N3-Cu-N3* 158.51(10)	N4-Cu-N7 157.37(8)	O7-Cu-N3 174.7(2)
N6-Cu-N3 89.54(6)	O1-Cu-N1 104.68(10)	N4-Cu1-N6 108.43(18)	N1-Cu-N2 79.40(10)	N4-Cu-N1 101.23(5)	N1-Cu-N7 88.61(7)	N1-Cu-N3 82.21(19)
N1-Cu-N5 89.23(6)	N4-Cu-N1 160.85(11)	N1-Cu1-N6 107.98(17)	N3-Cu-N2 81.19(10)	N2-Cu-N1 78.77(5)	N4-Cu-N6 90.46(7)	N4-Cu-N3 82.22(19)
N6-Cu-N5 84.18(6)	N2-Cu-N1 84.84(10)	N8-Cu1-N4 112.7(2)	N6-Cu-N1 127.90(11)	N3-Cu-N1 91.60(6)	N1-Cu-N6 156.55(8)	O7-Cu-N1 96.13(18)
N3-Cu-N5 153.36(6)	O1-Cu-N3 95.26(9)	N8-Cu1-N1 108.80(19)	N6-Cu-N3 119.11(11)	N3*-Cu-N1 92.57(6)	N7-Cu-N6 83.06(7)	O7-Cu-N4 99.37(19)
N1-Cu-O1 101.41(6)	N4-Cu-N3 101.19(10)			N4-Cu-N1* 101.23(5)	N4-Cu-N8 103.51(8)	
N6-Cu-O1 98.91(6)	N2-Cu-N3 77.94(10)			N2-Cu-N1* 78.77(5)	N1-Cu-N8 105.82(8)	
N3-Cu-O1 100.82(6)	N1-Cu-N3 87.81(9)			N1-Cu-N1* 157.54(10)	N7-Cu-N8 98.82(8)	
N5-Cu-O1 105.72(6)	O1-Cu-N4 91.41(10)			N4-Cu-N2 180.0	N6-Cu-N8 97.12(8)	
N1-Cu-N7 79.72(6)				N4-Cu-N3 79.25(5)	N4-Cu-N3 79.08(7)	
N6-Cu-N7 79.98(6)					N1-Cu-N3 79.59(7)	
N3-Cu-N7 78.21(6)					N7-Cu-N3 78.34(7)	
N5-Cu-N7 75.21(6)					N6-Cu-N3 77.27(7)	
O1-Cu-N7 178.51(6)					N8-Cu-N3 173.92(7)	

10.1002/ejic.202000488

Variable temperature $_1$H NMR studies

Room temperature $_1$H NMR spectra of **L$_1$** and **L$_2$** have been reported, as well as some of their diamagnetic metal complexes.[3,4] To determine the behavior in solution of both [**L$_1$**Cu$_I$(CH$_3$CN)]OTf and [**L$_2$**Cu$_I$(CH$_3$CN)]OTf, variable temperature (VT) $_1$H NMR spectroscopic studies were undertaken in anhydrous CD$_3$CN under N$_2$ from -30°C to 40°C. This technique was also employed as a tool to evaluate the reactivity of the Cu(I) complexes towards dry trimethylamine *N*-oxide (Me$_3$NO) as a potential oxygen-transfer agent. The spectrum of [**L$_1$**Cu$_I$(CH$_3$CN)]OTf shows a broad singlet for the methylene groups in the temperature range studied at δ 4.25, in agreement with a symmetric structure where both benzimidazole groups coordinate to the Cu(I) ion, as observed in the solid state (Figure 3). All the signals broaden at higher temperature, such that the methine and the *o*-pyridine H signals practically disappear at 40°C. The signal that presents the most drastic changes in chemical shift corresponds to the *m*-pyridyl H atoms, which shift from δ 7.07 to approximately 7.20 ppm, Figure 6a.

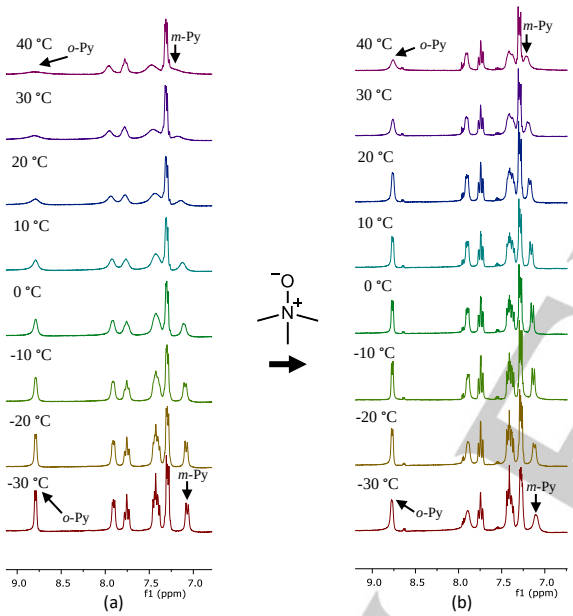

Figure 6. VT $_1$H NMR spectra of (a) aromatic region of [**L$_1$**Cu$_I$(CH$_3$CN)]OTf, and (b) after addition of Me$_3$NO in acetonitrile-*d*$_3$.

In the presence of a slight excess (1.3 equivs.) of Me$_3$NO, all signals are visible even at 40°C (Figure 6b); this difference can be attributed to the formation of a more rigid structure in the presence of Me$_3$NO as exogenous ligand. In the aliphatic region a similar behavior is observed, but the broad singlet at δ 3.93 that probably corresponds to Me$_3$NO bound to the metal center shifts to higher field with increasing temperature, and disappears at -10°C, see Figure S5 in the ESI. The presence of a small amount of a second, unidentified species is discernible in Figure 6b.

In contrast, VT $_1$H NMR spectra of [**L$_2$**Cu$_I$(CH$_3$CN)]OTf display more changes in the aliphatic region, with two broad singlets for the methylene H atoms at δ 4.63 and 4.03 observed at low temperature. The signals coalesce around -10°C, probably due to a fluxional process where only one quinoline group is bound to Cu(I) at low temperature, and rapid exchange between the two quinoline groups at higher temperature (Figure 7a),[20] although we cannot rule out the possibility of dimerization contributing to the fluxional process.[21] In the presence of excess Me$_3$NO (2.2 equivs.) required for full conversion, there is only one broad methylene signal even at low temperature, probably due to a faster exchange of both quinoline moieties. Although this is not clear at -30°C (compare Figure 7a with 7b), at -20°C the differences are well defined, since above that temperature the methylene groups give rise to a singlet at δ 4.29 in Figure 7b. A new singlet shifts from δ 4.16 to 3.65 over the range of -30°C to 10°C, which is consistent with fluxional behavior of Me$_3$NO; the signal shifts due to shielding by the Cu(I) ion (Figure 7b). Notably, an additional signal appears near that of the residual solvent protons at all temperatures (δ 1.96 in Figures 7 and S7), which can be assigned to the acetonitrile molecule competing with Me$_3$NO as exogenous ligand towards Cu(I), as observed in the solid-state structure, see Figure 4.

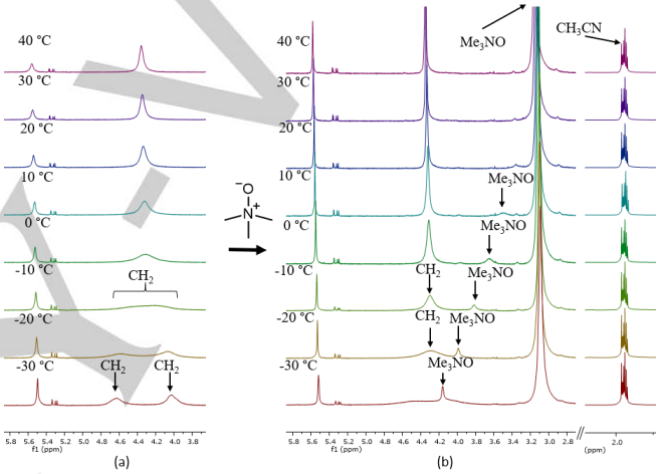

Figure 7. VT $_1$H NMR spectra of (a) aliphatic region of [**L$_2$**Cu$_I$(CH$_3$CN)]OTf, and (b) after addition of Me$_3$NO in acetonitrile-*d*$_3$.

As expected for the labile Cu(I) centers, the coordination mode differs in solution relative to that observed in the solid state, likely facilitated by the distorted tetrahedral geometry that contributes to the fluxional process,[22] considering also that the Cu-N$_{amine}$ interaction in [**L$_1$**Cu$_I$(CH$_3$CN)]OTf is weak. Temperature-dependent dynamic processes involve all *N*-donors of **L$_1$** and **L$_2$**, as well as acetonitrile and Me$_3$NO when present, consistent with Cu(I)-ONMe$_3$ adduct formation. The difference between both complexes can be attributed to the weaker donor ability of the quinoline ligand that accounts for the chemical shift differences observed for the methylene groups. In [**L$_1$**Cu$_I$(CH$_3$CN)]OTf, both benzimidazole fragments remain coordinated to the Cu(I) ion, based on the single resonance observed at all temperatures examined.

Since addition of Me$_3$NO to both Cu(I) complexes results in adduct formation with the *N*-oxide up to 40 °C, the reactions were monitored at 50 °C by $_1$H NMR during 80 min. Although the spectra are quite similar to those of the original complexes, formation of trimethyl amine was observed. The rate of formation is clearly larger in the presence of the quinoline-based derivative [**L$_2$**Cu$_I$(CH$_3$CN)]OTf (Figure 8), and also more selective (only one new signal appears at δ 2.13) than that of the benzimidazole derivative [**L$_1$**Cu$_I$(CH$_3$CN)]OTf (two new singlets at δ 2.13 and 2.16). The former signal is assigned to Me$_3$N, while the latter one

10.1002/ejic.202000488

may arise from the hydroxylated trimethylamine Me_2NCH_2OH, see Scheme 2. The chemical shift difference of 0.03 ppm is similar to that measured in the hydroxylation of *p*-cyano-*N*,*N*-dimethylaniline to *p*-cyano-*N*-hydroxymethyl-*N*-methylaniline (0.05 ppm).[10] The singlet observed at δ 1.96 for [**L**$_2$Cu$_I$(CH$_3$CN)]OTf disappears at 50 °C, so that the substitution of the coordinated acetonitrile molecule is complete at that temperature, something that was not observed at 40 °C in the VT experiments. The order of the reaction as well as the kinetic constants could not be obtained from these data due to the slow rate even at 50 °C, and the apparent order appears to change after longer reaction times.

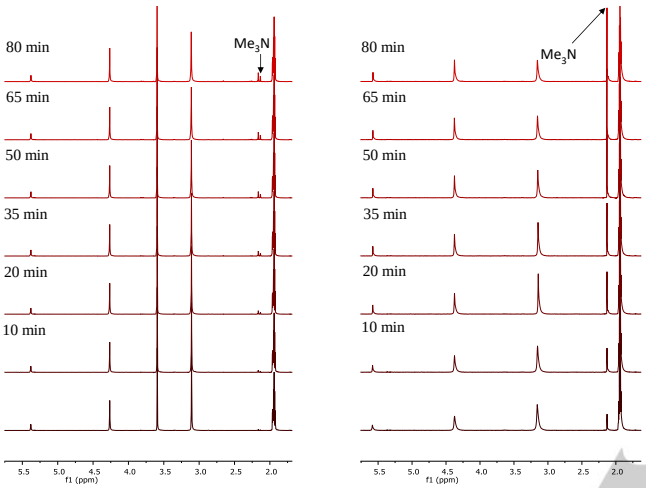

Figure 8. $_1$H NMR spectra of the aliphatic regions of (a) [**L**$_1$Cu$_I$(CH$_3$CN)]OTf, and (b) [**L**$_2$Cu$_I$(CH$_3$CN)]OTf at 50 °C in acetonitrile-d_3 after addition of Me$_3$NO, with formation of Me$_3$N.

Figure S8 in the ESI shows the $_1$H NMR spectrum of the product of the reaction between [**L**$_1$Cu$_I$(CH$_3$CN)]OTf and Me$_3$NO after several days, with only one new *o*-pyridyl signal at δ 8.64, as well as two methylene and one methyl singlet at δ 4.06 and 3.85 ppm, respectively. In contrast, the quinoline derivative [**L**$_2$Cu$_I$(CH$_3$CN)]OTf gives rise to a mixture of products, based on the numerous aromatic signals observed by $_1$H NMR spectroscopy in Figure S9. Lability of the pyridine based ligands in coordinatively saturated Cu(I) complexes has been proposed in atom transfer radical additions, where dissociation of one arm is a key step prior to homolytic cleavage of carbon-halogen bonds.[21] In other systems, however, O_2 binding and activation may be hampered by this dynamic behavior.[23]

UV-vis measurements

Optical spectroscopy measurements were carried out in acetonitrile to gain insight on the temperature-dependent coordination behavior of Me$_3$NO, which was analyzed at room temperature (RT) and -30 °C, although only minor changes were observed at low temperature. The spectra of the reaction between [**L**$_1$Cu(CH$_3$CN)]OTf and Me$_3$NO at room temperature is shown in Figure 9, at least three new bands appear at 235, 242, and 250 nm, which must correspond to a single product based on the $_1$H NMR spectroscopic observations (Figure S8). The UV-vis spectra of Me$_3$NO has been previously reported.[24],[25] In acetonitrile, Me$_3$NO presents an absorption band at 198 nm that has been assigned to a $n \rightarrow \sigma^*$ transition. Its basic character results in a hypsochromic shift in the presence of protic solvents or acids due to hydrogen bonding.

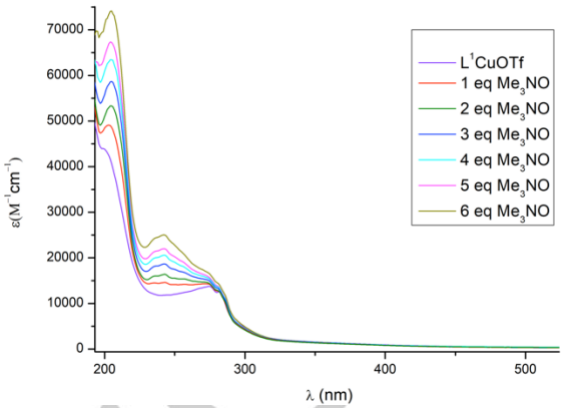

Figure 9. RT UV-vis spectra of 1 mM [**L**$_1$Cu$_I$(CH$_3$CN)]OTf and Me$_3$NO in acetonitrile.

Previous reports of the reactions of copper(I) complexes with *N*-oxide reagents indicate that the adducts are likely the initial products, but subsequent formation of Cu(III)$_2$(μ-O)$_2$ species may proceed with strongly electron-donating ligands.[9] The UV-vis spectrum of [**L**$_2$Cu$_I$(CH$_3$CN)]OTf at room temperature in Figure 10 shows absorption bands at 202 nm and 230 nm, and a shoulder around 268 nm. The band at 202 nm shifts to 206 nm, and a new shoulder appears at 262 nm in the presence of Me$_3$NO; these changes are more evident when an excess of the *N*-oxide is added (5 equivs.). This equilibrium[26] is reflected in the increase of the absorptivity at 206 nm, which does not correspond to the linear combination of the absorptivities of the reagents; the changes are evident after a few hours at 60 °C in the presence of 4 equivs. of Me$_3$NO. When a more concentrated solution of [**L**$_2$Cu$_I$(CH$_3$CN)]OTf is used, the appearance of two more bands is evident at 407 and 386 nm (ε = 940 and 1100 M^{-1}cm^{-1}, inset in Figure 10). Tolman and coworkers obtained a bis(μ-oxido)dicopper intermediate with a band at 423 nm,[9] generated from a related Cu(I)/β-diketiminate with Me$_3$NO as oxido transfer agent. Although the new bands could be tentatively assigned to a copper(III)-oxygen charge transfer band, the absorptivity reported is larger for the diketiminate-based analog. Thus, the bands at 407 and 386 nm must correspond to one of the final Cu(II) oxidation products, rather than a copper-oxygen intermediate since a μ–oxido species is not expected to be stable at 60 °C.

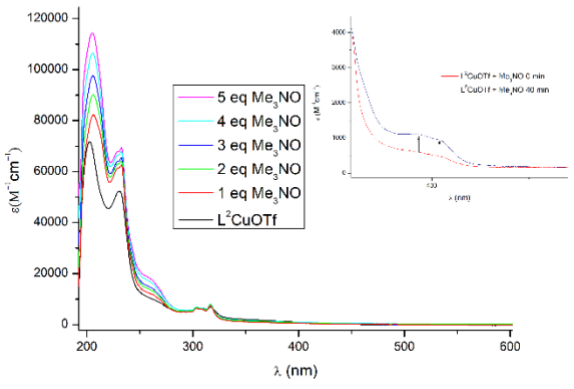

Figure 10. RT UV-vis spectra of 1 mM [**L**$_2$Cu$_I$(CH$_3$CN)]OTf and Me$_3$NO in acetonitrile. Inset: spectra acquired at 60 °C.

EPR measurements

The changes that occur during the reactions between [**L**$_{1,2}$Cu^{I}(CH$_3$CN)]OTf and 3 equivs. of Me$_3$NO at room temperature in acetonitrile were interrogated by variable temperature Electron Paramagnetic Resonance (EPR) experiments after immediately freezing the sample, to determine the presence of radical species. Further analysis was carried out by analyzing the samples by mass spectrometry (MS). In the reaction of [**L**$_1$Cu^{I}(CH$_3$CN)]OTf, a small amount of Cu(II) species with axial geometry is present from -160 °C to -100 °C. The intensity increases from -100 °C to -60 °C, and more signals are evident (Figure S10). Thus, at elevated temperature oxidation of [**L**$_1$Cu^{I}(CH$_3$CN)]OTf to a mixture of Cu(II) species becomes evident. Analysis of the organic products by DART MS revealed the presence of a small amount of di(2-pyridyl)ketone (*m/z* = 185 [M+H]$^+$) as oxidation product. The spectrum of the main component observed at -60 °C in Figures 11 and S11 was simulated with $g_{\parallel}$ = 2.35, $A_{\parallel}$ = 12.22 mT. This *g* value is larger than the one measured for [**L**$_1$Cu^{II}(CH$_3$CN)]OTf$_2$ ($g_{\parallel}$ = 2.29, $A_{\parallel}$ = 14.88 mT) in the initial stages of the reaction with Me$_3$NO. Coordination of an oxygen donor should increase the value of $g_{\parallel}$ and decrease that of $A_{\parallel}$ due to the poorer σ-donor capability of oxygen relative to nitrogen from acetonitrile,[28] supporting the formation of a cupric species [**L**$_1$Cu^{II}(S)]$^{2+}$ with S = oxygen donor, Me$_3$NO or OH$^-$ (see below). This interaction between an exogenous O-donor and the Cu(II) center is also evidenced in the hyperfine coupling in Figures S10 and S11, since the spectra of both initial Cu(II) complexes [**L**$_1$Cu^{II}(H$_2$O)](NO$_3$)$_2$ and [**L**$_2$Cu^{II}(NO$_3$)]NO$_3$ are nearly isotropic (Figure S12). At the end of the reaction, complex [**L**$_1$Cu^{II}(CH$_3$CN)]OTf$_2$ was isolated as the main copper(II) product, albeit only in 33% yield, see below.

The reaction between [**L**$_2$Cu^{I}(CH$_3$CN)]OTf and 3 equivs. of Me$_3$NO at 50 °C for one hour was also monitored by EPR at 77 K, although in this case a very low intensity isotropic signal was observed at all temperatures. This corresponds to the presence of a small amount of Cu(II) present, most probably from decomposition to the bis(diquinolinecarboxamide) cupric complex in Figure 5. The reaction was also analyzed by DART MS, showing the formation of a considerably larger amount of di(2-pyridyl) ketone than in the case of **L**$_1$.

Reaction of the corresponding copper(II) complexes with Me$_3$NO at room temperature results in decrease of the EPR signals (Figure S13). Further analysis by Electrospray mass spectrometry (ESI MS) of [**L**$_1$Cu^{II}(H$_2$O)](NO$_3$)$_2$ after addition of Me$_3$NO resulted in a base peak at *m/z* = 536, assigned to [**L**$_1$Cu]$^+$ (Figure S14); interestingly, the peak at *m/z* = 571 agrees with the proposed formulation [**L**$_1$Cu^{II}(OH)(H$_2$O)]$^+$, which may arise from heterolytic oxido-transfer from Me$_3$NO, followed by H-abstraction; the cupric-hydroxo species may dimerize, accounting for its EPR-silent nature. A similar behavior has been reported in the reactions of Cu(II) complexes with Me$_3$NO, where heterolytic oxido transfer with concomitant loss of the radical cation Me$_3$N$^{\bullet+}$ was proposed.[8],[27] Antiferromagnetically coupled Cu(II)$_2$ or oxido-bridged Cu(III)$_2$ species could form as end products, but no experimental evidence was obtained by MS. In the case of [**L**$_2$Cu(NO$_3$)]NO$_3$, FAB$^+$ MS shows an increase in the intensity of the cation at *m/z* = 530 assigned to [**L**$_2$Cu^{I}]$^+$ after addition of Me$_3$NO, relative to the peak at *m/z* = 592 for [**L**$_2$Cu^{II}(NO$_3$)]$^+$ (Figure S15).

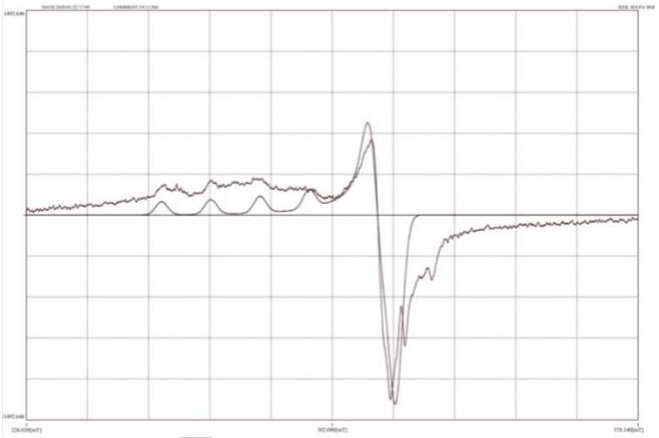

Figure 11. EPR spectrum of the reaction between [**L**$_1$Cu^{I}(CH$_3$CN)]OTf and Me$_3$NO in acetonitrile at -60 °C; simulation of the main component shown as smooth line.

Cyclic voltammetry

The electrochemical properties of the complexes were investigated by cyclic voltammetry. The voltammograms obtained in anodic direction for [**L**$_1$Cu^{I}(CH$_3$CN)]OTf and [**L**$_2$Cu^{I}(CH$_3$CN)]OTf are shown in Figure 12, with the former one showing an irreversible process for the Cu$^{II/I}$ redox couple with cathodic and anodic peaks E_{cp} = -521 and E_{ap} = -284 mV. The peak difference ($\Delta E_p = E_{pa} - E_{pc}$) corresponds to 237 mV at a scan rate of 100 mV s^{-1}, while ΔE for the reference ferrocenium/ferrocene (Fc$^{+/0}$) under the same conditions is 71 mV. The quinoline-based derivative [**L**$_2$Cu(CH$_3$CN)]OTf is characterized by a quasi-reversible process with $E_{1/2}$ = -260 mV vs Fc$^{+/0}$ (ΔE_p = 114 mV, see Figure 12). The values of the half-wave potentials obtained contrast with the reactivity described above: [**L**$_1$Cu(CH$_3$CN)]OTf with a more negative potential is expected be more reactive towards oxidants than [**L**$_2$Cu(CH$_3$CN)]OTf, including dioxygen. Nonetheless, only [**L**$_2$Cu(CH$_3$CN)]OTf is oxidized in THF solution by air to afford bis(2-quinolinecarboxamidato)copper(II). This apparent kinetic control of the reactivity may be related to the higher lability of the quinoline fragment, as established by VT ^{1}H NMR spectroscopy.

The potential values determined agree with the lower basicity of the quinoline fragment, and consequently its lower σ-donor ability, compared to that of benzimidazole.[4],[15] Both complexes present an irreversible reduction process at -2.47 and -2.07 V, respectively, which is attributed to the reduction to metallic copper that deposits on the electrode surface (Figure S16). This is consistent with the presence of a wave at -0.70 V for the reoxidation of metallic copper in both complexes (formation of Cu^0 complexes is rare),[29] and by changing the switching potential to a more positive value, which makes the oxidation wave disappear. Finally, their stability was tested in the presence of water, with a water content of 5% by volume having virtually no effect on the voltammograms.

10.1002/ejic.202000488

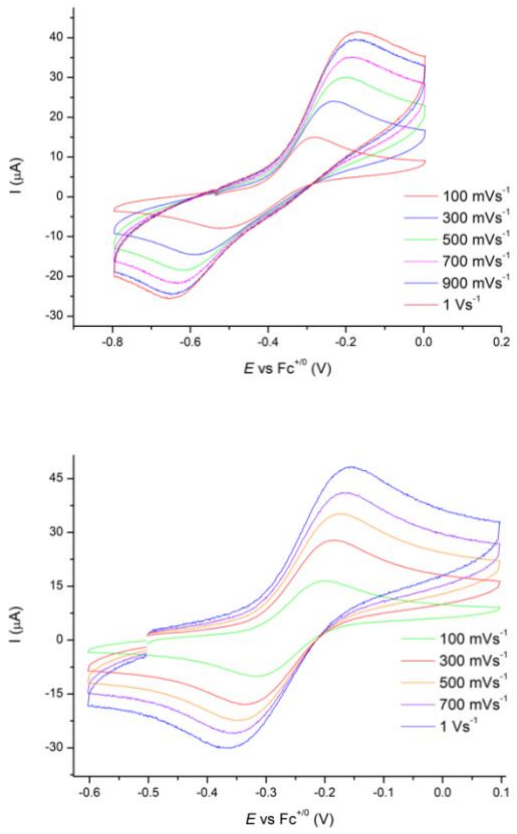

Figure 12. Cyclic Voltammograms of [**L**$_1$Cu^{I}(CH$_3$CN)]OTf (above), and [**L**$_2$Cu^{I}(CH$_3$CN)]OTf (below) at different scan rates in acetonitrile, 1 mM solution using [NBu$_4$]ClO$_4$ as a supporting electrolyte, *E* vs Fc$^{+/0}$ (V).

Preparative scale reactions with Me$_3$NO

Large scale reactions of [**L**$_1$Cu^{I}(CH$_3$CN)]OTf with 2 equivs. of Me$_3$NO resulted in two isolable products that were amenable for crystallization, their solid-state structures are shown in Figure 13. The first one corresponds to the cupric analogue [**L**$_1$Cu^{II}(CH$_3$CN)]$^{2+}$ that features intact **L**$_1$, isolated in 33% yield; the second one corresponds to the fragment bis(1*H*-benzimidazole-2)methanamine (**L**$_4$) as ligand in [**L**$_4$Cu^{II}(OTf)$_2$(H$_2$O)], Figure 13. This species was also detected by ESI-MS, and isolated in 5% yield. The second fragment expected from the oxidation of **L**$_2$ corresponds to di(2-pyridyl)ketone, which was detected by comparative thin layer chromatographic analysis with an authentic sample, and confirmed by DART MS (Figure S17).

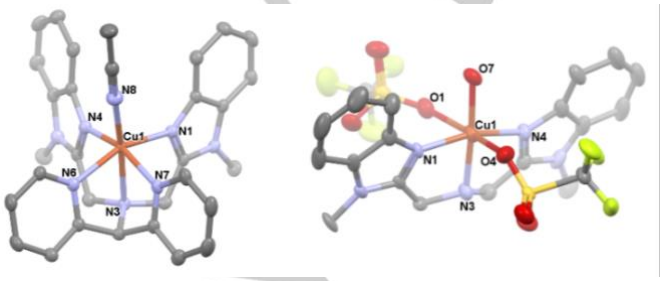

Figure 13. Mercury diagrams of [**L**$_1$Cu^{II}(CH$_3$CN)]$^{2+}$ (left), and [**L**$_4$Cu^{II}(OTf)$_2$(H$_2$O)] (right) at the 50% probability level; H atoms, solvent molecules, and non-coordinating triflates are omitted for clarity.

[**L**$_1$Cu^{II}(CH$_3$CN)]OTf$_2$ presents an elongated *pseudo*-octahedral geometry, formally with a *C*$_s$ point symmetry; the Cu-N(*sp*$_2$) distances are shorter [2.000(2) to 2.090(2) Å], while the Cu-N3 distance of 2.351(2) Å to the central amine is the longest. This structure is quite similar to the aqua complex in Figure 2, with the most remarkable differences being the smaller angle between the axial donors (N3-Cu-N8 173.92° *vs* N7-Cu-O1 178.51°), and the pyridyl-Cu-amine bite angles (78.34° and 77.27° in [**L**$_1$Cu^{II}(CH$_3$CN)]$^{2+}$ *vs* 79.98° and 75.21° in [**L**$_1$Cu^{II}(H$_2$O)]$^{2+}$). Such differences might be the consequence of the higher ligand field strength of acetonitrile[30] (and a larger Jahn-Teller distortion), and/or hydrogen bonding of the water ligand in [**L**$_1$Cu^{II}(H$_2$O)]$^{2+}$ with nitrate counter ions (O-H...O distances of 2.73 and 2.76 Å). In the case of [**L**$_4$Cu^{II}(OTf)$_2$(H$_2$O)], the point symmetry corresponds to *C*$_{2v}$ in a *pseudo*-octahedral geometry, with the two oxygen atoms of the triflate anions in axial positions. The Cu-N bond lengths corresponding to the benzimidazole donors are shorter, as expected, at 1.992(6) and 1.972(6) Å. The Cu-N3 distance of 2.032(4) Å is slightly longer due to its formally N(*sp*$_3$) nature, while the Cu-O7 bond towards the water molecule in equatorial position is the shortest of the Cu-O bonds at 1.926(4) Å.

The reaction between [**L**$_2$Cu^{I}(CH$_3$CN)]OTf and 2 equivs. of Me$_3$NO afforded [(**L**$_3$)$_2$Cu^{II}] in 20% yield, this complex was also obtained upon slow oxidation of the cuprous complex in the presence of air. The isolated yields are in agreement with the observations made by ^{1}H NMR (Figure 8b), showing the formation of Me$_3$N by oxygen atom transfer mainly to **L**$_2$, which would require excess Me$_3$NO for full conversion of **L**$_2$ to **L**$_3$. This may occur by initial O-atom transfer to the Cu^{+} center, with concomitant formation of the putative Cu(II)-oxyl intermediate that can mediate intra- or intermolecular C-H activation of the dipyridylmethyne fragment. In contrast, the reaction of [**L**$_1$Cu^{I}(CH$_3$CN)]OTf leads predominantly to its cupric analogue [**L**$_1$Cu^{II}(CH$_3$CN)]OTf$_2$, indicating that intramolecular C-H activation is not the only manifold accessible, as confirmed by the small amount of dipyridylketone detected. Additionally, Me$_3$N was formed along with a byproduct based on ^{1}H NMR spectroscopy, which may correspond to hydroxylation of the trimethylamine to form dimethylaminomethanol (see Scheme 2). Control reactions of both **L**$_1$ and **L**$_2$ with equimolar amounts of Me$_3$NO in acetonitrile at 50 °C resulted in no changes after 12 h based on TLC analysis, confirming that oxygen transfer from the amine *N*-oxide is copper-mediated.

10.1002/ejic.202000488

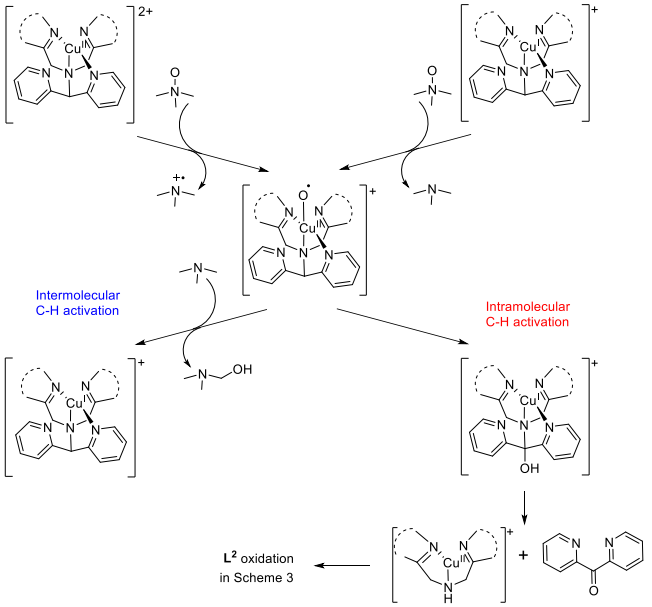

Scheme 2. Proposed mechanism of inter- and intramolecular C-H activations *via* putative Cu(II)-oxyl intermediate.

Similarly, [**L**$_2$Cu$_I$(CH$_3$CN)]OTf and Me$_3$NO may interact in the same way according to the products observed, but with further oxidation of the corresponding bis(quinoline)amine fragment to yield the bis(2-quinolinecarboxamidato)copper(II) complex [(**L**$_3$)$_2$Cu$_{II}$], as shown in Scheme 3. Finally, ESI MS analysis of the mixtures of [**L**$_1$Cu$_I$(CH$_3$CN)]OTf and larger amounts of Me$_3$NO (4 equivs.) after heating in acetonitrile at 50 °C for two h resulted in the observation of a cationic species at *m/z* = 653, assigned to [**L**$_1$Cu(CH$_3$CN)(Me$_3$NO)+H]$_+$ (Figure S18). Moreover, the species detected at *m/z* = 571 and 462 were assigned to Cu(II)-OH species, consistent with H-abstraction. In the case of [**L**$_2$Cu$_I$(CH$_3$CN)]OTf, the species detected at *m/z* = 633 was assigned to [(**L**$_3$)Cu(Me$_3$NO)]$_+$ (Figure S19).

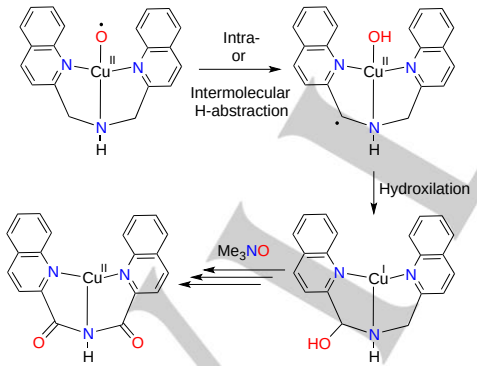

Scheme 3. Copper-mediated sequential oxidation of **L**$_2$ to afford **L**$_3$.

Attempts to isolate the proposed Me$_3$NO adducts by evaporation of volatiles, followed by washing with diethylether, resulted in brown-red solids that were analyzed by IR spectroscopy as KBr pellets. Information about the coordination of Me$_3$NO was not forthcoming, since aliphatic amine oxides in general do not show appreciable changes in the N-O bond vibration when oxygen is bound to a metal ion. Indeed, the bond distance in coordinated complexes does not change significatively from that of free Me$_3$NO or in the hydrochloride.[31] In the case of aromatic amine *N*-oxides a shift is expected as an effect of the change in the contribution of the resonance structures, but they are not expected for their aliphatic counterparts.[32]

Conclusion

The reactivity of Me$_3$NO with Cu(I) complexes supported by the potentially pentadentate **L**$_1$ and **L**$_2$ is consistent with initial adduct formation, with the copper(I) complexes being oxidized slowly to copper(II) species. VT ^{1}H NMR confirmed the interaction between the Me$_3$NO and the Cu(I) complexes, while EPR experiments evidenced the formation of paramagnetic Cu(II) species from [**L**$_1$Cu$_I$(CH$_3$CN)]OTf and Me$_3$NO at the beginning of the reaction, although EPR-silent species are present among the final products, based on the quantification of the Cu(II) complexes isolated. The determined redox potentials contrast with the observed stability of the complexes toward oxidants like dioxygen and Me$_3$NO, which leads us to postulate that the rate and selectivity of the oxidation products are controlled by kinetic factors, with the higher lability of the *N*-donors in the [**L**$_2$Cu$_I$(CH$_3$CN)]OTf system resulting in a less hindered and more reactive species. Finally, the observed inter- and intramolecular C-H activations must occur through reactive copper-oxygen complexes that were not detected, but that could reasonably correspond to a bis(μ-oxido)dicopper(III) species, or the proposed Cu(II)-oxyl as intermediates.

Experimental Section

Reagents and techniques

Reagents and solvents were obtained from commercial sources. Trimethylamine-*N*-oxide dihydrate was dried by sublimation under reduced pressure. All reactions and manipulations were carried out under dinitrogen atmosphere using an MBraun glove box or standard Schlenk techniques. IR spectra were acquired with a Perkin Elmer 203-B FT-IR spectrophotometer in the range of 4000–400 cm^{-1} as KBr pellets. ^{1}H and ^{13}C NMR spectra were recorded with a JEOL Eclipse 300 spectrometer. Fast Atom Bombardment mass spectra (FAB) were measured on a JEOL JMS-SX-102A spectrometer, and electrospray ionization mass spectra (ESI) were acquired with a Bruker Daltonics Esquire 6000 spectrometer with an ion trap. For both [**L**$_1$Cu(H$_2$O)](NO$_3$)$_2$ and [**L**$_2$Cu(NO$_3$)]NO$_3$, ESI mass spectra were recorded on a Waters QTOF XEVO-G2 spectrometer as MeCN solutions. Electron Paramagnetic Resonance (EPR) spectra were recorded on a JEOL JES- TE300 spectrometer in quartz tubes at X band frequency (9.4 GHz) at 77 K as frozen solutions. Spectra were simulated with the ES-PRITS-TE software from JEOL Ltd.

Crystal Structure Determinations

Suitable single crystals of the studied compounds were mounted on a glass fiber; crystallographic data of [**L**$_1$Cu$_{II}$(H$_2$O)](NO$_3$)$_2$ and [**L**$_2$Cu$_{II}$(NO$_3$)]NO$_3$ were collected with a Rigaku Oxford Diffraction Supernova diffractometer at 120 K using λ(Mo K$_\alpha$) = 0.71073 Å. Cell refinement and data reduction were performed with the CrysAlisPro software.[33] The structures were solved by the charge flipping method using the Superflip program.[34] Data for the other crystals were collected on an Oxford Diffraction Gemini "A" diffractometer with a CCD area detector, λ(CuK$_\alpha$) = 1.54184 Å for [**L**$_2$Cu$_I$(CH$_3$CN)]OTf, [(**L**$_3$)$_2$Cu$_{II}$], and λ(Mo K$_\alpha$) = 0.71073 Å for [**L**$_1$Cu$_I$(CH$_3$CN)]OTf, [**L**$_4$Cu$_{II}$(OTf)$_2$(H$_2$O)], and [**L**$_1$Cu$_{II}$(CH$_3$CN)](OTf)$_2$, at 130 K. Unit cell parameters were determined with a set of three runs of 15 frames (1° in ω). The double pass method of scanning was used to exclude noise.[33] The collected frames were

integrated by using an orientation matrix determined from the narrow frame scans. Final cell constants were determined by a global refinement; collected data were corrected for absorbance by using analytical numeric absorption correction using a multifaceted crystal model based on expressions upon the Laue symmetry with equivalent reflections.[35] Structure solutions and refinements were carried out with the SHELXS-2014[36] and SHELXL-2014[37] packages. WinGX v2018.3[38] software was used to prepare material for publication. Full-matrix least-squares refinement was carried out by minimizing $(Fo^2 - Fc^2)^2$. All non-hydrogen atoms were refined anisotropically. H atoms of the water molecule (H–O) were located in a difference map and refined isotropically with $U_{iso}(H) = 1.5$ for H–O. H atoms attached to C atoms were placed in geometrically idealized positions and refined as riding on their parent atoms, with C–H = 0.95 – 1.00 Å and with $U_{iso}(H) = 1.2U_{eq}(C)$ for aromatic, methylene and methine groups, and $1.5U_{eq}(C)$ for methyl groups. Crystallographic data for all complexes are presented in Tables S1 and S2 in the Electronic Supporting Information (ESI). Crystallographic data for the structures reported in this paper has been deposited with the Cambridge Crystallographic Data Centre as supplementary publication nos. CCDC 1983674-1983680. Copies of the data can be obtained free of charge on application to CCDC, 12 Union Road, Cambridge, CB2 1EZ, UK (fax: (+44) 1223-336-033, e-mail: deposit@ccdc.cam.ac.uk).

Synthetic procedures

Synthesis of {[N,N-bis(1-methyl-2-benzimidazolylmethyl)-N-(bis-2-pyridyl)methylamine]copper(II)} nitrate

[*N,N*-bis(1-methyl-2-benzimidazolylmethyl)-*N*-(bis-2-pyridyl)methylamine] (**L1**) was synthesized by the procedure previously reported.[4] To a solution of **L1** (100 mg, 0.21 mmol) in 3 mL of acetonitrile was added a solution of $Cu(NO_3)_2{\cdot}3H_2O$ (51 mg, 0.21 mmol) in 2 mL of acetonitrile. The resulting mixture was allowed to stir for 6 h at room temperature under inert atmosphere and the greenish blue reaction mixture was reduced to *ca.* 3 mL upon slow evaporation. The resulting concentrated acetonitrile solution was placed into an ethyl acetate bath for slow vapor diffusion and stored for five days to grow single crystals suitable for X-ray crystallographic analysis. The obtained crystals were washed with ethyl acetate and dried under vacuum to afford solid product in 78% yield (112 mg). UV-Vis in CH_3CN: λ_{max}, nm (ε, M^{-1} cm^{-1}): 668 (41), 374 (117). HR ESI MS: $[\mathbf{L_1}Cu(NO_3)]^+$ *m/z* = 598.1516 (calc. 598.1502).

Synthesis of {[N,N-bis(2-quinolylmethyl)-N-bis(2-pyridyl)methylamine]copper(II)} nitrate[3]

Ligand [*N*,*N*-bis(2-quinolylmethyl)-*N*-bis(2-pyridyl)methylamine] (**L2**) was synthesized by the procedure previously reported. To a solution of ligand **L2** (100 mg, 0.21 mmol) in 3 mL of acetonitrile was combined with a solution of $Cu(NO_3)_2{\cdot}3H_2O$ (52 mg, 0.21 mmol) in 2 mL of acetonitrile. The resulting mixture was allowed to stir for 6 h at room temperature under inert atmosphere and the turquoise color reaction mixture was left to evaporate to *ca.* 3 mL upon slow evaporation. The resulting concentrated acetonitrile solution was placed into an ethyl acetate bath for slow vapor diffusion and stored for five days to afford single crystals suitable for X-ray diffraction analysis. The crystals were washed with ethyl acetate, dried under vacuum. Yield: 117 mg (83%). UV-Vis in CH_3CN: λ_{max}, nm (ε, M^{-1} cm^{-1}): 699 (27), 372 (59). HR ESI MS: $[\mathbf{L_2}Cu(NO_3)]^+$ *m/z* = 592.1288 (calc. 592.1284).

Synthesis of {[N,N-bis(1-methyl-2-benzimidazolylmethyl)-N-(bis-2-pyridyl)methylamine]copper} trifluoromethanesulfonate

Ligand **L1** (100 mg, 0.21 mmol) was dissolved in anhydrous acetonitrile and $[Cu(CH_3CN)_4]OTf$ (79 mg, 0.21 mmol) was added to the solution and stirred for 2 h. Crystals were obtained by slow evaporation of the reaction mixture and cooling to -30 °C. The complex was isolated as yellow crystals in 90% yield (130 mg, 0.19 mmol). M.p. 182-183 °C. ^{1}H NMR ($CDCl_3$, 300 MHz): δ 8.79 (s, 2 H, *o*-Py), δ 7.93 (s, 2 H, *p*-Py), δ 7.76 (t, 2 H, J = 7.3 Hz, *m*-Py), δ 7.43 (s, 4 H, BzIm-H), δ 7.34-7.27 (m, 4 H, BzIm-H), δ 7.15 (s, 2 H, *m*-Py-H), δ 5.34 (s, 1 H, CH), δ 4.25 (s, 4 H, CH_2), δ 3.59 (s, 6 H, NCH_3). IR (KBr) ν_{max}/cm^{-1}: 3081(w), 2942(w), 2880(w), 2837(w), 2814(w), 1589(m), 1569(w), 1480(m), 1462(m), 1452(m), 1433(m), 1325(w), 1284(w), 1246(vs), 1221(s), 1147(vs), 1099(s), 1029(vs), 1007(w), 976(w), 962(w), 938(w), 921(w), 883(m), 849(w), 790(w), 766(s), 750(vs), 700(w), 682(w), 634(vs), 607(w), 568(m), 549(w), 515(s), 446(w), 437(w), 417(w). ESI MS *m/z* (rel. intensity): 536 ($[(\mathbf{L_1}Cu)]^+$, 32%), 474 ($[\mathbf{L_1}+H]^+$, 39%). Anal. Calcd. for $C_{30}H_{27}CuF_3N_7O_3S$ (%): C, 52.51; H, 3.97; N, 14.29; S, 4.67. Found: C, 52.91; H, 3.97; N, 14.34; S, 4.32.

Synthesis of {[N,N-bis(2-quinolylmethyl)-N-bis(2-pyridyl)methylamine]copper} trifluoromethanesulfonate

Ligand **L2** (100 mg, 0.21 mmol) was dissolved in anhydrous acetonitrile, $[Cu(CH_3CN)_4]OTf$ (80 mg, 0.21 mmol) was added to the solution, and stirred for 2 h. Crystals were obtained by slow evaporation of mixture reaction or keeping a concentrated acetonitrile solution at -30 °C. The complex was isolated as orange crystals in 90% yield (130 mg, 0.19 mmol). M.p. 122-123 °C. ^{1}H NMR ($CDCl_3$, 300 MHz): δ 8.60 (m, 4 H, *o*-Py, *p*-Q), δ 8.20 (d, 2 H, *J* = 8.46, Q), δ 7.87 (t, 4 H, *J* = 7.65, Q, *m*-Py), δ 7.72 (t, 2 H, *J* = 7.62, *p*-Py), δ 7.63-7.58 (m, 2 H, *J* = 8.46, Q), δ 7.43 (s, 2 H, Q), δ 7.32 (s, 4 H, Q, *m*-Py), δ 5.55 (s, 1 H, CH), δ 4.34 (s, 4 H, CH_2). IR (KBr) ν_{max}/cm^{-1}: 3064(w), 3019(w), 1618(w), 1596(m), 1567(w), 1508(m), 1469(m), 1437(m), 1370(w), 1305(w), 1255(vs), 1223(s), 1147(s), 1121(m), 1099(w), 1055(w), 1028(vs), 996(w), 977(w), 958(m), 918(w), 893(w), 842(w), 822(m), 784(s), 755(s), 689(w), 633(vs), 593(w), 571(m), 515(s), 493(m), 485(w), 416(w), 405(w). ESI MS *m/z* (rel. intensity): 530 ($[(\mathbf{L_2}Cu)]^+$, 100%). Anal. Calcd. for $C_{32}H_{25}CuF_3N_5O_3S$ (%): C, 56.51; H, 3.70; N, 10.30; S, 4.71. Found: C, 56.19; H, 3.66; N, 10.21; S, 3.93.

Acknowledgements

The authors thank María de los Angeles Peña for NMR spectroscopy, Lucero Ríos and Carmen Márquez for mass spectrometry, Virginia Gómez-Vidales for EPR measurements, Rocío Patiño-Maya for IR spectroscopy, María de la Paz Orta for combustion analysis, Conacyt (A1-S-8682, beca 294604) and DGAPA-PAPIIT (IN203317, IN217020) for financial support.

Keywords: Copper; oxido transfer; nitrogen ligands; C-H activation; oxidation

[1] K. Ray, F. F. Pfaff, B. Wang, W. Nam, *J. Am. Chem. Soc.* **2014**, *136*, 13942–58.

[2] C. E. Elwell, N. L. Gagnon, B. D. Neisen, D. Dhar, A. D. Spaeth, G. M. Yee, W. B. Tolman, *Chem. Rev.* **2017**, *117*, 2059–2107.

[3] W. K. C. Lo, C. J. McAdam, A. G. Blackman, J. D. Crowley, D. A. McMorran, *Inorg. Chim. Acta* **2015**, *426*, 183–194.

[4] M. Mitra, H. Nimir, S. Demeshko, S. S. Bhat, S. O. Malinkin, M. Haukka, J. Lloret-Fillol, G. C. Lisensky, F. Meyer, A. A. Shteinman, et al., *Inorg. Chem.* **2015**, *54*, 7152–7164.

[5] N. Gagnon, W. B. Tolman, *Acc. Chem. Res.* **2015**, *48*, 2126–2131.

[6] Y. Shimoyama, T. Kojima, *Inorg. Chem.* **2019**, *58*, 9517–9542.

[7] M. Srnec, R. Navrátil, E. Andris, J. Jašík, J. Roithová, *Angew. Chem. Int. Ed.* **2018**, *1*, 1–6.

[8] P. Capdevielle, D. Sparfel, J. Baranne-Lafont, N. K. Cuong, M. Maumy, *J. Chem. Soc. Chem. Commun.* **1990**, *565*, 565.

[9] S. Hong, A. K. Gupta, W. B. Tolman, *Inorg. Chem.* **2009**, *48*, 6323–6325.

[10] D. E. Diaz, M. Bhadra, K. D. Karlin, *Inorg. Chem.* **2019**, *58*, 13746–13750.

[11] J. R. Winkler, H. B. Gray, in *Mol. Electron. Struct. Transit. Met. Complexes*, Springer, Berlin, **2011**, pp. 17–28.

[12] B. J. Hathaway, in *Inorg. Chem.*, Springer-Verlag, Berlin/Heidelberg, **2005**, pp. 49–67.

[13] A. A. Massie, M. C. Denler, R. Singh, A. Sinha, E. Nordlander, T. A. Jackson, *Chem. Eur. J.* **2020**, *26*, 900–912.

[14] W. Rasheed, A. Draksharapu, S. Banerjee, V. G. Young, R. Fan, Y. Guo, M. Ozerov, J. Nehrkorn, J. Krzystek, J. Telser, et al., *Angew. Chem. Int. Ed.* **2018**, *57*, 9387–9391.

[15] M. Lõkov, S. Tshepelevitsh, A. Heering, P. G. Plieger, R. Vianello, I. Leito, *Eur. J. Org. Chem.* **2017**, 4475–4489.

[16] C. E. Elwell, B. D. Neisen, W. B. Tolman, *Inorg. Chim. Acta* **2019**, *485*, 131–139.

[17] R. Sahu, S. K. Padhi, H. S. Jena, V. Manivannan, *Inorg. Chim. Acta* **2010**, *363*, 1448–1454.

[18] J. M. Rowland, M. M. Olmstead, P. K. Mascharak, *Inorg. Chem.* **2002**, *41*, 2754–2760.

[19] S. K. Padhi, V. Manivannan, *Inorg. Chem.* **2006**, *45*, 7994–7996.

[20] D. A. K. Coggin, J. A. González, A. M. Kook, L. J. Wilson, D. M. Stanbury, *Inorg. Chem.* **1991**, *30*, 1115–1125.

[21] W. T. Eckenhoff, A. B. Biernesser, T. Pintauer, *Inorg. Chem.* **2012**, *51*, 11917–11929.

[22] A. Bheemaraju, J. W. Beattie, Y. Danylyuk, J. Rochford, S. Groysman, *Eur. J. Inorg. Chem.* **2014**, *2014*, 5865–5873.

[23] E. W. Dahl, H. T. Dong, N. K. Szymczak, *Chem. Commun.* **2018**, *54*, 892–895.

[24] T. Mukai, *Nippon kagaku zassi* **2011**, *79*, 1547–1551.

[25] M. Yamakawa, T. Kubota, H. Akazawa, *Theor. Chim. Acta* **1969**, *15*, 244–264.

[26] L. Chmurzynski, Z. Pawlak, H. Myszka, *J. Mol. Struct.* **1982**, *80*, 235–242.

[27] P. Comba, S. Knoppe, B. Martin, G. Rajaraman, C. Rolli, B. Shapiro, T. Stork, *Chem. Eur. J.* **2008**, *14*, 344–357.

[28] J. Peisach, W. E. Blumberg, *Arch. Biochem. Biophys.* **1974**, *165*, 691–708.

[29] R. R. Conry, *Encycl. Inorg. Chem.* **2006**, 1–19.

[30] M. A. Halcrow, *Chem. Soc. Rev.* **2013**, *42*, 1784–1795.

[31] P. A. Giguère, D. Chin, *Can. J. Chem.* **1961**, *39*, 1214–1220.

[32] T.-Y. Luh, *Coord. Chem. Rev.* **1984**, *60*, 255–276.

[33] 2013. CrysAlisPro, version 1.171.36.32; Oxford Diffraction Ltd.: Abingdon, U.K.

[34] L. Palatinus, G. Chapuis, *J. Appl. Crystallogr.* **2007**, *40*, 786–790.

[35] R. C. Clark, J. S. Reid, *Acta Crystallogr. Sect. A* **1995**, *51*, 887–897.

[36] G. M. Sheldrick, *Acta Crystallogr. Sect. A Found. Crystallogr.* **2015**, *71*, 3–8.

[37] G. M. Sheldrick, *Acta Crystallogr. Sect. C Struct. Chem.* **2015**, *71*, 3–8.

[38] L. J. Farrugia, *J. Appl. Crystallogr.* **2012**, *45*, 849–854.

10.1002/ejic.202000488

Entry for the Table of Contents

Copper-oxygen species

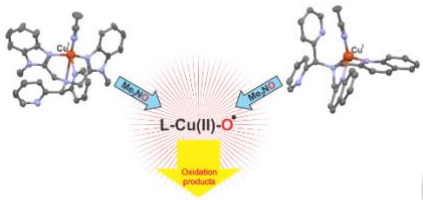

Cu(I) complexes with pentadentate benzimidazole- and quinoline-based ligands react with trimethylamine *N*-oxide to afford Cu(I)-ONMe$_3$ adducts, and subsequently intra- and intermolecular oxidation products. Although spectroscopic evidence of the reactive copper-oxygen intermediates was not forthcoming, the reaction appears to proceed through a putative copper(II)-oxyl species.

Researcher Twitter: @IvanCas68860420